

# Indium doped zinc oxide nanopowders for transparent conducting coatings on glass substrates

Naji Al Dahoudi · Amal AlKahlout ·  
Sabina Heusing · Petra Herbeck-Engel ·  
Rudolf Karos · Peter Oliveira

Received: 4 May 2013 / Accepted: 7 July 2013 / Published online: 17 July 2013  
© Springer Science+Business Media New York 2013

**Abstract** Crystalline indium doped zinc oxide (IZO) nanopowders were synthesized using hydrothermal treatment processing. Increasing the doping ratio of indium in the zinc oxide significantly influences the phase structure and shape of the nanopowders resulting in nanorod to nanoparticulate morphologies. As the doping profile increases, the crystallite size decreases, the band gap energy blue shifts and the specific surface area increases (measured by BET method). Additionally Raman spectroscopy exhibited shifts of several peaks, as well as revealed new peaks, confirming the substitution of indium ions within the zinc oxide lattice sites. An IZO suspension made of IZO nanoparticles (In/Zn = 3 atm.%) with a zeta potential greater than 30 mV at pH = 6 was successfully spin-coated on glass substrates for to make transparent conductive coatings evincing sheet resistances as low as  $35 \text{ k}\Omega_{\square}$  ( $\rho = 4.9 \times 10^{-3} \Omega \text{ m}$ .) with transmission in the visible range as high as 90 %.

**Keywords** Indium doped zinc oxide · Transparent conducting oxides · Spin coating · XRD · SEM · Raman spectroscopy

## 1 Introduction

Zinc oxide, as a wide band gap semiconductor of band gap of 3.37 eV, with a high exciton binding energy of 60 meV and its high electron mobility makes it technologically important. So that it is intensively studied and widely used in multidisciplinary applications, such as in solar energy conversion, thin film transistors, catalysis, nonlinear optics, gas sensors, pigments, cosmetic, etc. [1–13]. Nanostructured size zinc oxide can be found in different forms, like nanoparticles, nanorods, nanobelts, nanoflowers, etc. [14–18]. Doping zinc oxide with some elements like aluminum, gallium, boron, niobium and indium [19–23] have a great impact for enhancing the optical, electrical, thermal and magnetic properties. Indium doped Zinc oxide (IZO) nanostructured materials are considered a favorable nanomaterial for transparent conducting layers [24] gas sensors [25] and photodetectors due to their promising opto-electrical properties [26].

The electrical properties of transparent conducting electrodes depend mainly on the charge carrier density as well as their mobility. The increase of the charge carrier density can be achieved by deviating the stoichiometry, owing to oxygen deficiency, which is normally obtained by a reducing treatment, or by doping the host lattice with substitutive materials (cationic or anionic). It is well known that the electrical conductivity of ZnO-based TCOs can be significantly improved via the incorporation of aluminium [27, 28] gallium [29] or indium [30, 31]. The mobility of the charge carriers is strongly influenced by the disorder in the crystal structure resulting from the modification of the crystalline periodicity due to doping. It is therefore strongly affected by the different scattering processes of free charge carriers.

The use of sols, made of well crystalline dispersed conductive nanoparticles, realize thick films with high

N. Al Dahoudi (✉) · A. AlKahlout  
Physics Department, Al Azhar University-Gaza,  
P.O. Box 1277, Gaza, Palestine  
e-mail: naji@alazhar.edu.ps

S. Heusing · P. Herbeck-Engel · R. Karos · P. Oliveira  
INM—Leibniz-Institut für Neue Materialien GmbH,  
Campus D2 2, 66123 Saarbrücken, Germany

transparency; however a very high thermal energy is needed to sinter the particles. A stable colloid is required to produce a single layer with reasonable thickness using wet chemical deposition techniques. However, the production of thick films in a single step is still a challenge.

Most reports in literature regarding wet chemical methods for preparing metal-doped zinc oxide films concern sol-gel method. Sol-gel method is a low cost and attractive wet-chemical approach for TCO films preparation when sheet resistance is not of prime importance. One of the drawbacks of this technique is the need for drying and heat treatment at relatively high temperature to convert the gel hydroxide film into an oxide phase. This step is energy consuming and not suitable to many kinds of substrates. In addition, numerous deposition-calcination cycles are needed. Deposition using colloidal suspension of already crystalline nanoparticles is another interesting option, in which the crystallization step of the TCO material is separated from the process of film formation. It is worth mentioning that synthesis of transparent conductive coating starting with low cost materials like crystalline ZnO nanoparticles with simple steps will be a significant achievement for the industry to coat many kinds of substrates especially formed glasses and polymeric substrates.

In this work indium doped zinc oxide nanopowders were synthesized using hydrothermal processing for different indium doping concentrations. The resulting nanopowders were successfully dispersed in an organic solvent to produce transparent conductive layers on a glass substrate. The optical, electrical and structural properties of the obtained IZO nanopowders and layers were studied.

## 2 Experimental work

### 2.1 IZO nanopowder synthesis

The Indium-doped Zinc Oxide (IZO) nanopowders were synthesized using the precipitation and the growth process in a liquid phase during a hydrothermal processing technique. The precursor solution was prepared by dissolving 18 g of zinc nitrate hexahydrate in 2-methoxyethanol as a solvent, and stirred for 30 min till a clear solution is obtained. The indium content was controlled by the change in the atomic ratio of ethanolic solution of indium nitrate to the zinc solution from 0 to 5 atm.%. The resultant solution was heated up to 60 °C for 30 min under stirring, and then an aqueous solution of sodium hydroxide (3 M) is slowly added dropwise to the former solution under vigorous stirring. A white suspension is formed and left under stirring for 6 h at the same temperature (60 °C). The pH of the solution is then adjusted between 11 and 13. The solution is then cooled down to RT and kept stirring for 2 h to yield a

homogeneous solution. The solution was transferred to hydrothermal treatment process at 200 °C for 6 h. The obtained powder is then washed with bidistilled water and centrifuged at 4,000 rpm for 30 min several times. Then the resulted white powder is dried at 100 °C for 24 h. The dried material is grinded using a hammer mill to reduce the size of the agglomerates until a fine powder is obtained.

### 2.2 IZO coating sol

The IZO powder is wetted in a small amount of a mixture of polyethylene glycol (PEG) and trioxadecneic acid (TODS), where PEG/TODS is 3:1 in weight. The amount of TODS is adjusted to get a stable suspension at a pH value of 6. The wetted powder is grinded by hand for 10 min using a hammer mortar to obtain a homogeneous paste. The resulted paste is dissolved in 1-propanol, sonicated for 5 min in an ultrasonic bath, and then centrifuged at 4,000 rpm for 10 min to remove the large remaining agglomerates. The solid content of the IZO coating sol is 5 wt %.

### 2.3 Deposition technique

The prepared coating sol was used directly to be deposited on borosilicate and quartz substrates using spin coating technique. The spinning parameters were spinning speed of 1,000 rpm for 20 s. The wet layer is directly sintered in oven at 600 °C for 15 min in air. For obtaining multilayers, the single step spinning with the sintering process is repeated several times. At the end, a sintering process for 30 min at 600 °C was carried out, followed by a post annealing treatment in reducing atmosphere (forming gas N<sub>2</sub>: H<sub>2</sub> = 98:2) at temperatures between 300 and 500 °C for 90 min.

### 2.4 IZO nano-powder, sol and coatings characterization

The obtained IZO nanopowders with different doping concentrations were characterized to determine the phase structure and the crystallite size using X-ray Powder Diffractometer, SIEMENS Type D500 employing a CuK $\alpha$  radiation ( $\lambda = 15,418 \text{ \AA}$ ) source and equipped with a 25 kV power. The crystallite size was calculated using Scherrer equation. The specific (BET) surface area were also determined at the saturation vapour pressure of liquid nitrogen using an ASAP 2400, Micromeritics equipment. The morphology of the nanopowders as well as the surface morphology were imaged using a high-resolution scanning electron microscopy FR-SEM (JSM6400F, JEOL) using the secondary electron signal excited by a 10 keV primary beam. The nanopowder structure were investigated using a

transmission electron microscope (HRTEM-CM200 FEG, Philips). The transmission, and absorption of the nano-suspensions were measured using a CARY 5E UV–VIS–NIR spectrophotometer from Varian. The measurements were carried out within the range 300–3,000 nm. All measurements were done at room temperature. To investigate the local vibration modes Raman spectra was measured using the Raman spectrometer LabRAM ARAMIS.

The zeta potential of the coating solution was measured using an Acoustosizer II equipment, Colloidal Dynamics by titration of the sol.

The thermal behaviour of the sols and the coated materials obtained after different post deposition treatments were examined simultaneously by differential thermal analysis and thermogravimetry (TG) up to 1,000 °C at a rate of 10 °C per minute using a Bähr Gerätbau, STA501 equipment.

The sheet resistance ( $R_{\square}$ ) of the films was measured using the four-point probe technique. The electrical resistivity ( $\rho$ ) of the layers were calculated from the formula,  $\rho = R_{\square}t$  where  $t$  is the layer thickness.

### 3 Result and discussion

#### 3.1 Phase and structural properties

##### 3.1.1 XRD

Figure 1 shows the X-ray diffraction patterns of IZO nanopowders with different indium concentrations from 0 to 5 atm.%. The pattern depicted a decrease of the intensity of the main peaks, more broadening of the peaks by increasing the doping concentration. By monitoring the position and the FWHM of all the peaks in the pattern, it is found that the main peaks correspond to the polycrystalline hexagonal zincite structure of ZnO, which are indexed on the basis of JCPDS card no. 01-070-2551. A new significant peak at  $2\theta_{\square} = 22$ , which corresponds to the Dzhalindite, syn cubic  $\text{In}(\text{OH})_3$  phase, is found in the pattern. This peak is growing by increasing the indium doping concentration. This phase revealed that traces of new phases exist beside the zincite hexagonal ZnO structure. Furthermore, indium precursor with reactivity much higher than that of zinc precursor may also lead to individual nanocrystals with cubic structures [30].

A slight shift to lower diffraction angles, and a peak broadening are observed by increasing the concentration of the indium dopant from 0 to 5 mol %. The slight variation in the peak broadening and angle diffraction may be referred to the substitution of indium ions in the sites of  $\text{Zn}^{2+}$  [32]. The variation in the crystallite size are depicted

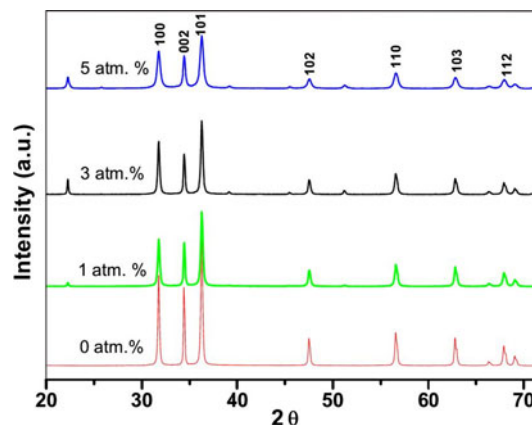


**Fig. 1** XRD patterns of dried pure and In doped ZnO powder with different In concentrations

in Table 1, where smaller grains are observed by increasing the In doping ratio.

##### 3.1.2 SEM and TEM

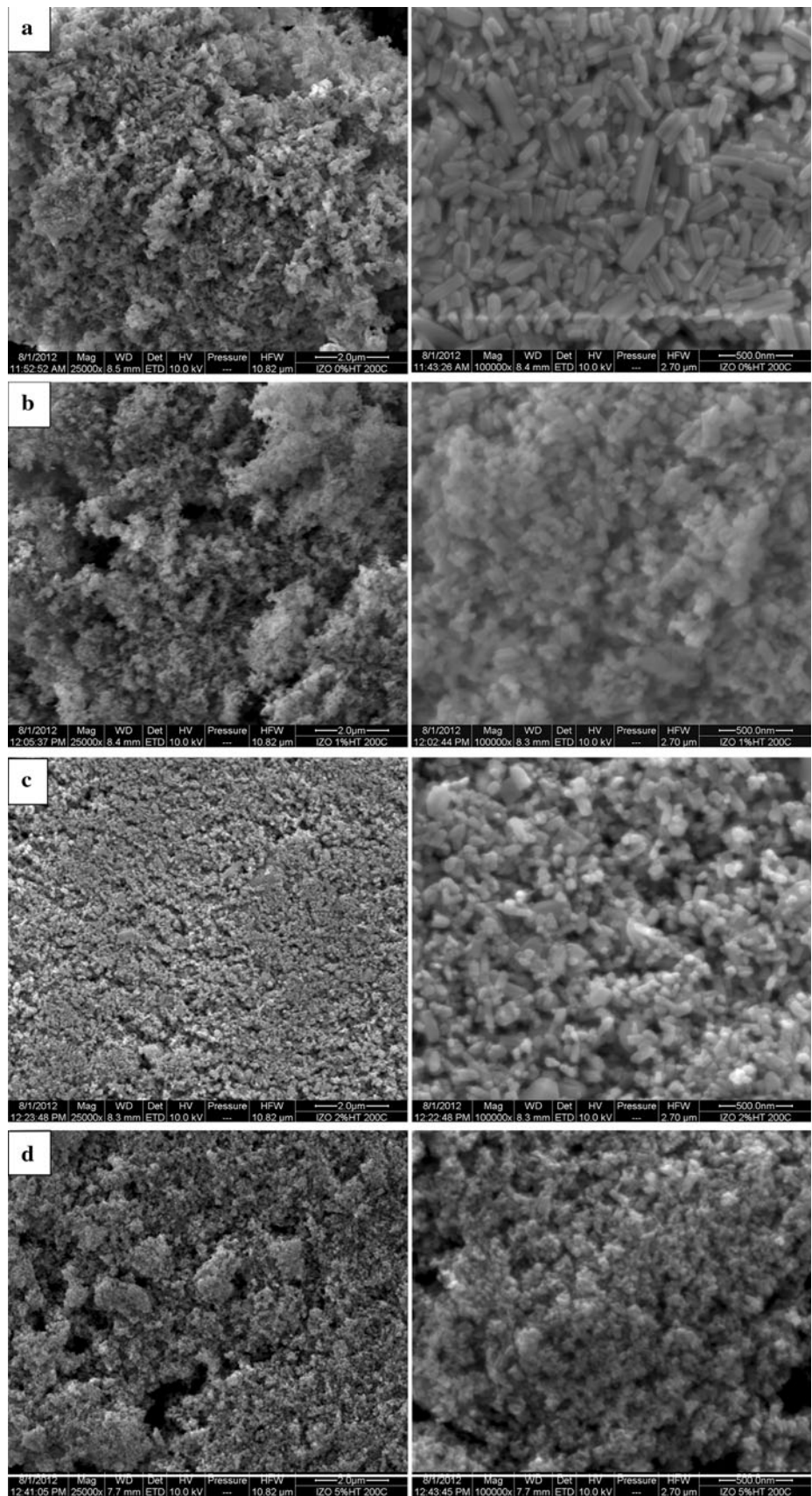
Figures 2 and 3 show the SEM and TEM morphology with different magnification of IZO nanopowders for different doping concentration. It is observed in Fig. 2a–d a remarkable dopant induced shape evolution in the case of increasing the doping ratio. The pure zinc oxide (Fig. 2a) exhibited a rod like shaped structure, where their lengths ranged from 70 to 300 nm and diameter between 30 and 60 nm. It is demonstrated that the incorporation of indium ions into the zinc oxide seeds affected the growth of the host lattice and the nanostructured form. The rod shape structure is shown for pure zinc oxide, which transforms gradually to spherical nanoparticulate shape. It is exhibited from the images, a reduction of the size of the nanoparticles by increasing the concentration of indium dopant, which is in agreement with the XRD data in Table 1.

The TEM images shown in Fig. 3 still appear the rodlike polycrystalline nanostructure of the pure zinc oxide nanopowder, which likely transformed to spherical nanostructure by doping the zinc oxide lattice. Figure 3b exhibited an aggregation of nanoparticles for the 5 atm.% indium doped zinc oxide sample with particle sizes distributed over a range between 20 and 50 nm.

**Table 1** The table shows the crystallite size as a function of the In concentration in IZO nanopowders as calculated from the zincite phase peaks

In doping concentration (atm.%)	Phase name	Crystallite size (nm)
0	Zincite	82
1	Zincite	56
3	Zincite	56
5	Zincite	29

**Fig. 2** SEM images with different magnifications of indium doped ZnO nanopowders for **a** 0, **b** 1, **c** 3 and **d** 5 atm.%



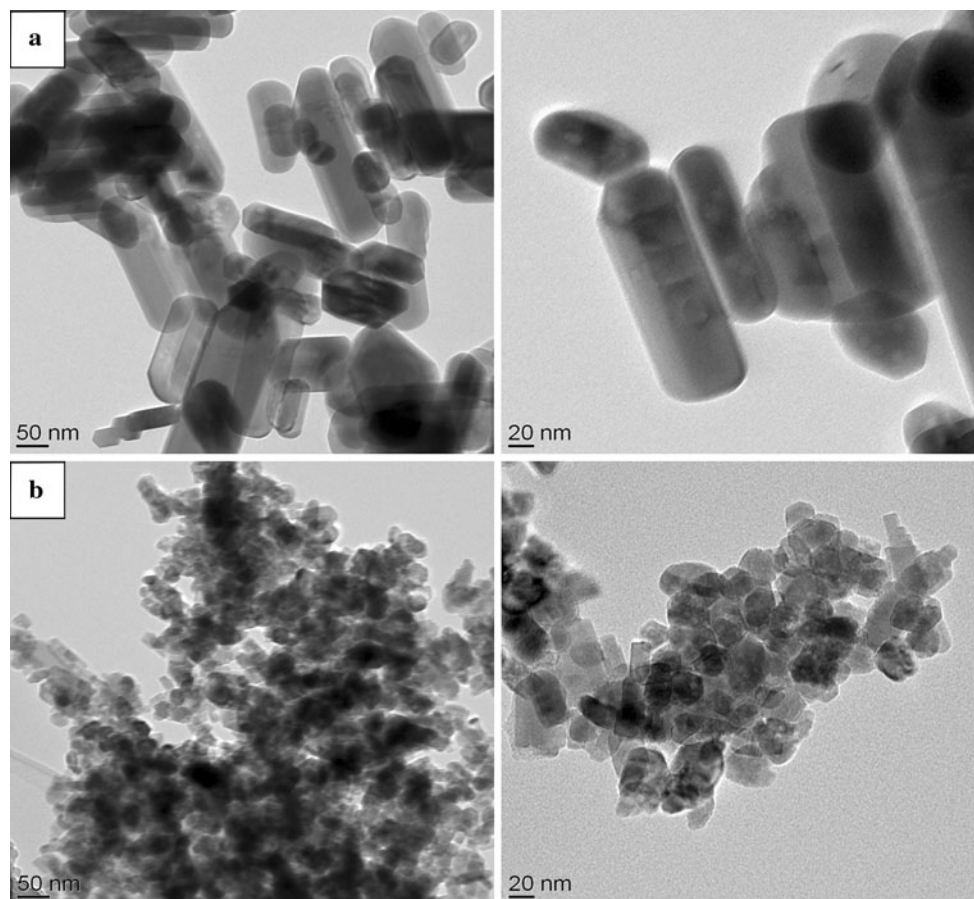


**Fig. 3** TEM images of the crystalline nanopowders redispersed in water **a** pure zinc oxide **b** 5 atm.% IZO with different magnification

### 3.1.3 UV-VIS Absorption

The energy gap of the synthesized pure and indium doped zinc oxide nanopowders was determined from their UV–VIS absorption spectra. Figure 4 (left) shows the absorption spectra of pure and In doped ZnO measured between 300 and 600 nm. The absorption edge of the spectra is shifted to a higher energy (blue shift) by doping the zinc oxide with indium ions, where a reduction of the particle size is observed. The blue shift of the absorption position can be assigned to the direct transition of electrons in the zinc oxide nanocrystals. The energy band gap ( $E_g$ ) values can be obtained from the absorption coefficient  $\alpha$ , which can be calculated as a function of the photon energy ( $h\nu$ ). The relationship between the absorption coefficient and photon energy can be expressed as [33].

$$(\alpha h\nu)^2 = C(h\nu - E_g)$$

where  $C$  is a constant.  $\alpha$  can be calculated from the expression  $\alpha = A/d$ , where  $A$  is the measured absorbance and  $d$  is the thickness of the sample in the UV–Vis cell. The  $E_g$  value can be obtained by extrapolating the linear portion of the graph of  $(\alpha h\nu)^2$  versus  $h\nu$ , which has been

shown in Fig 4 (right). The obtained value for pure zinc oxide is 3.16 eV and increased to 3.21 eV for In doping ratio of 1 atm.% and a further slight increase to 3.23 for In doping of 5 atm.%. These values of energy gap are smaller than that of 3.3 eV reported for single crystalline ZnO samples, which may be related to the presence of vacancies and dopants [34].

### 3.1.4 Raman spectroscopy

In order to check the influence of indium doping on zinc oxide, a Raman spectroscopy measurements were carried out at room temperature. Figure 5 exhibited the Raman spectra of the pure zinc oxide compared with the spectra of 3 and 5at.% of indium doped zinc oxide samples. The Raman spectrum from the pure ZnO nanopowder exhibited a well-defined narrow peak at  $440\text{ cm}^{-1}$  which is blue shifted by +3 to the assigned peak of the two  $E_2$  modes. This is in a good agreement with that of wurtzite ZnO [34]. The peaks at 334, 380, 480, 539, and  $656\text{ cm}^{-1}$  are related with a small shift to the  $E_2^{\text{high}}-E_2^{\text{low}}$ ,  $A_1(\text{TO})$ ,  $E_1(\text{TO})$ ,  $2B_1^{\text{low}}$  (2LA), and  $\text{TA} + \text{LO}$ , respectively [35]. Such bands are assigned as second order Raman spectrum arising

**Fig. 4** UV/VIS absorption of pure and indium doped zinc oxide nanopowders redispersed in ethanol (left) and  $(\alpha h\nu)^2$  versus the photon energy  $h\nu$  curve (right)

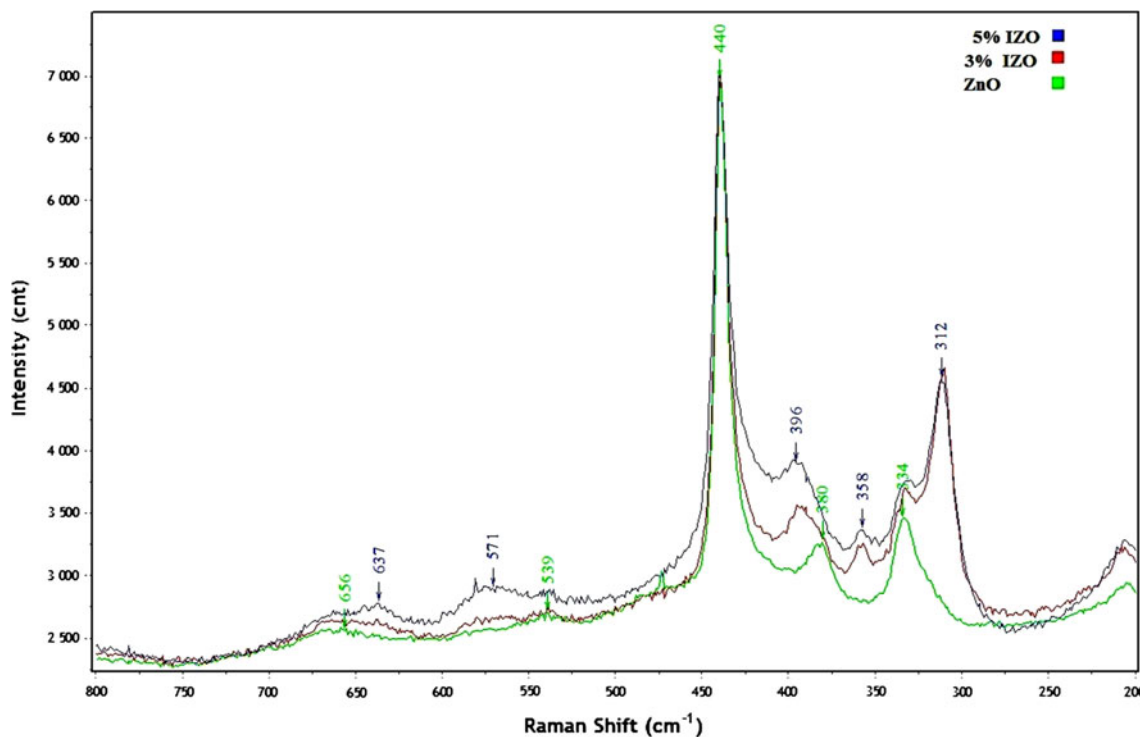
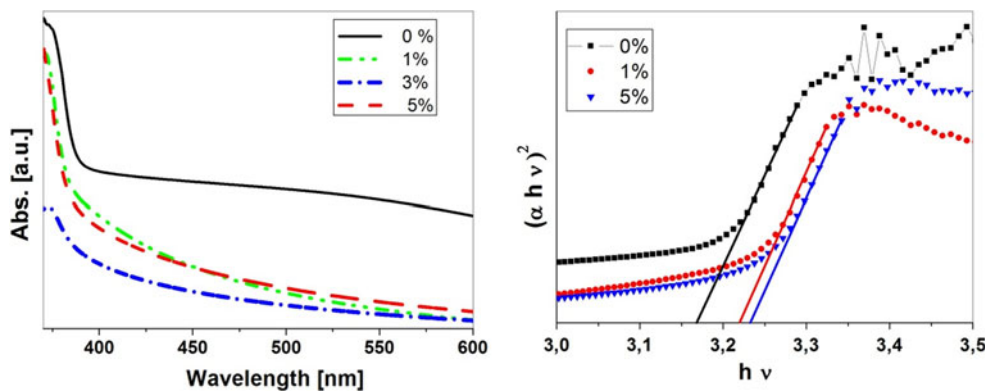


**Fig. 5** Raman spectrum of pure and indium doped zinc oxide nanopowders

from the zone boundary phonons. The shift in the peaks compared with the theoretical values may refer to the optical phonon confinement by the nanorod structure [36].

The Raman spectrum of indium doped zinc oxide samples revealed a shift of the peaks at 334, 380, 440  $\text{cm}^{-1}$  and a weakness of the peaks at 480, 539, and 656  $\text{cm}^{-1}$ , which related to the substitution of indium ions in the zinc oxide lattice. New additional vibration peaks at 312, 358, 396, 571 and 639  $\text{cm}^{-1}$  are shown assigned to the doped zinc oxide samples. According to some reports, the new peaks in the IZO samples, may be attributed to the indium impurities phases, which confirms the peaks revealed in the XRD patterns shown in Fig. 1 [37, 38].

### 3.1.5 BET Surface area

The surface area of the pure and indium doped zinc oxide nanopowders were measured. The results shown in Fig. 6 revealed the increase of the BET surface area of the samples as a function of the doping concentration. The gradual increase of the BET surface area from 11 to 16  $\text{m}^2/\text{g}$  by increasing the doping ratio from 0 to 3 atm.%, and a significant increase to 33  $\text{m}^2/\text{g}$  was observed for the sample of the 5 atm.% doping ratio. This is in consistent with the results of the measurements of the crystallite size given from the XRD pattern and the SEM images given in table 1 and Fig. 2.

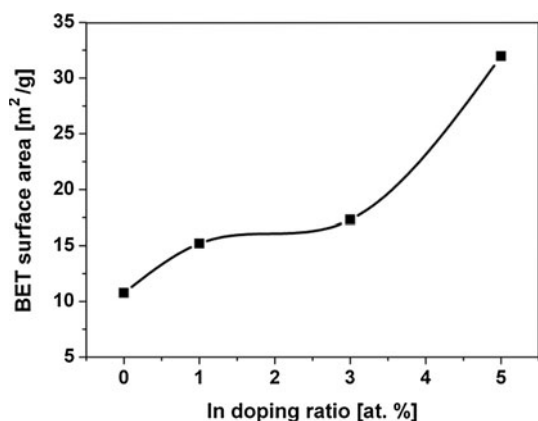


**Fig. 6** The BET surface area of IZO nanopowders as a function of indium doping concentration

## 3.2 Coating sol characterizations

### 3.2.1 Zeta potential

The measurement of the Zeta potential is a good index of the magnitude of the interaction between the colloidal particles and is used to assess the stability of a colloidal system as a function of the pH. The zeta potential of the colloidal sol was tested to check the the stability of the colloidal IZO nanoparticles in terms of the pH value as shown in Fig. 7. The surface of the IZO nanoparticle exhibited high zeta potential in both acidic and basic medium, which means that the repulsive force between the particles could overcome the Van der Waal forces. The isoelectric point (IEP) of the sol is 9.2, where the IEP of zinc oxide found in the literature ranges from 8.7 to 10.3 [39, 40]. So that a sol of pH = 6 is used for depositing transparent conducting layers on glass substrates in this work.

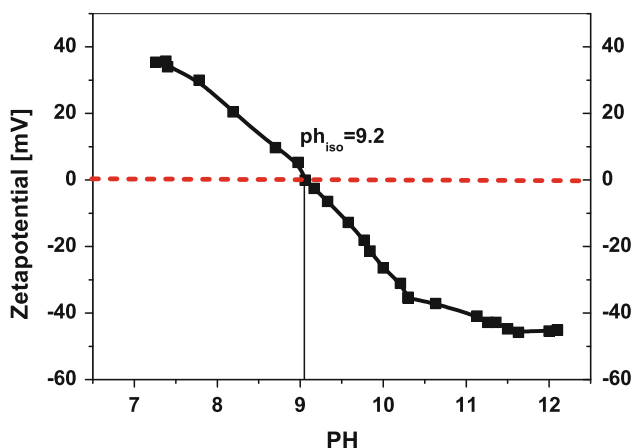


**Fig. 7** Zeta potential of IZO suspension as a function of pH

### 3.2.2 Thermal analysis

In order to better understand the components and thermal behavior of the as-synthesized coating sol composed of IZO nanoparticles (In: Zn = 3 atm.%) dispersed in PEG and the dispersive agent TODS, TG and DSC were carried out as shown in Fig. 8. The DSC thermograms of the as synthesized IZO paste showed a weak broaden exothermic peak centered at 180 °C corresponding with a weight loss of about 7 %. This loss may referred to the decomposition of the adsorbed OH species. An abrupt weight loss of more than 60 % is observed between 250 and 470 °C, accompanied by a wide exothermal peak centered at  $T = 346$  °C. This was as a result of the degradation of the organic groups of polyethylene glycol and the shoulder at  $T = 420$  °C is attributed to the decomposition of the TODS. At temperature greater than 500 °C, almost no extra weight loss is observed, which means that the removal of all organic species in the IZO paste. This indicates that no phase transition occurred at temperature higher than 500 °C.

## 3.3 Thin film characterizations

### 3.3.1 XRD

Figure 9 shows the X-ray diffraction patterns of ZnO thin films doped with indium (In/Zn: 3 atm.%) deposited on borosilicate glass and sintered at 600 °C. It can be seen from the pattern that all samples are polycrystalline and exhibit the single-phase ZnO hexagonal wurtzite structure. The peak intensities of the film are different from that of the particles shown in Fig. 1, where an increase of the growth into the [100] orientation more than the growth into the [002] orientation. This may referred as a result from the sintering of the nanoparticles, which indicates that heating

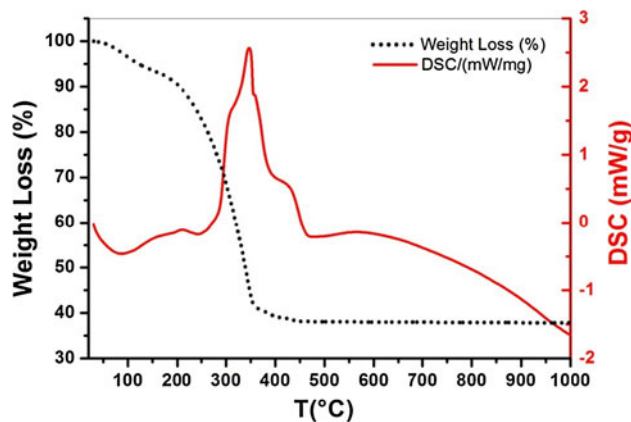


**Fig. 8** TG and DSC for IZO paste (In/Zn: 3 atm.%)

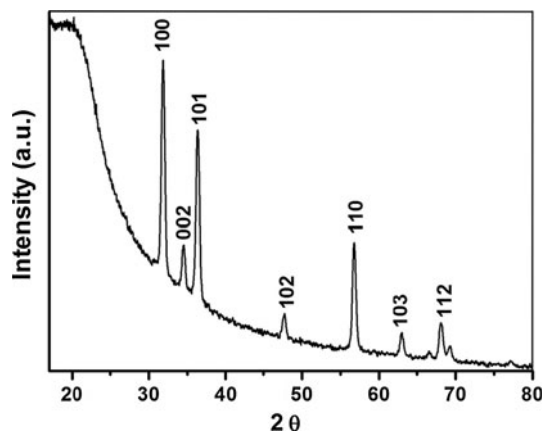


**Fig. 9** XRD pattern of spin coated IZO layer (In/Zn: 3 atm.%) deposited on borosilicate glass substrate and sintered at 600 °C

up to 600 °C deteriorates the crystallinity of the layers, which may be due to the formation of stress induced by ion size difference between zinc and indium and the segregation of indium ions in grain boundaries for high temperature sintering.

### 3.3.2 Electrical and optical properties

The electrical properties of indium doped zinc oxide coatings were characterised as a function of the doping concentration (Fig. 10). As shown, the electrical specific resistivity of spin coated IZO layer sintered in air at  $T = 600\text{ °C}$  first decreases with increasing In concentration, passes by a minimum at around 2–3 atm.% and then increases. Undoped zinc oxide layer has a high electrical resistivity,  $\rho = 55\text{ }\Omega\cdot\text{cm}$  ( $R_{\square} > 10\text{ M}\Omega_{\square}$ ). The minimum resistivity is about  $6 \times 10^{-1}\text{ }\Omega\cdot\text{cm}$  ( $R_{\square} = 92\text{ k}\Omega_{\square}$ ) at In concentration of 3 atm.%. It is expected that the reduction of resistivity of the layer by doping zinc oxide referred to the increase of the carrier concentration, which originated

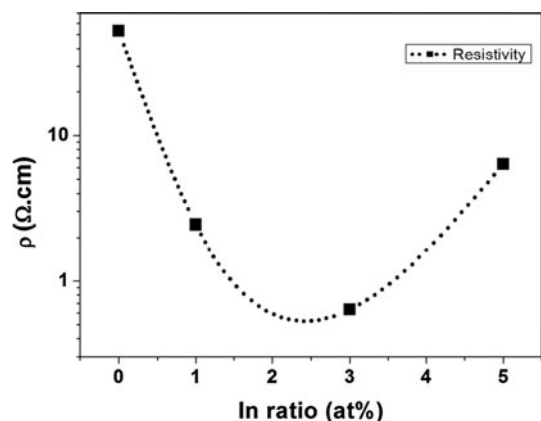


**Fig. 10** Specific electrical resistivity of spin coated IZO layer on borosilicate glass substrate sintered at 600 °C and followed by reducing in forming gas as a function of indium doping concentration

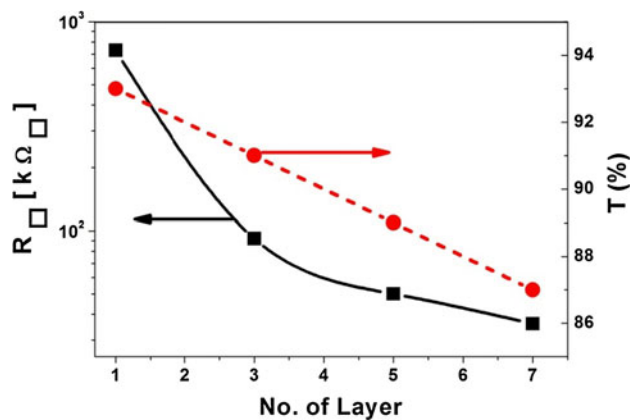


**Fig. 11** The sheet resistance and the transmittance at  $\lambda = 550\text{ nm}$  of spin coated multilayers of IZO (In: Zn: 3 tm. %)

from the substitution of  $\text{In}^{3+}$  ion for  $\text{Zn}^{2+}$  ion releases one electron in the lattice contributing to the conductivity. The resistivity of the film is raised to  $6.6\text{ }\Omega\cdot\text{cm}$  at 5 atm.% In concentration, which may as a result from the grain boundaries due to the smaller crystallite size. In addition to that, more indium concentration behaves like electron traps, which reduces the charge carrier concentration.

The sheet resistance of IZO layers were studied as a function of number of the layers sintered at 600 °C, and post annealed at 400 °C under forming gas as shown in Fig. 11. The sheet resistance of a single layer is high, almost  $1\text{ M}\Omega_{\square}$ , which decrease sharply by increasing the number of layers. A sheet Resistance as low as  $35\text{ k}\Omega_{\square}$  is measured for 7 layers. The multilayers still exhibited high transmittance between 93 to 86 % when the number of layers increased from 1 to 7.

Figure 12 shows the transmission spectra in the UV–VIS–NIR region for one, three and seven IZO layers

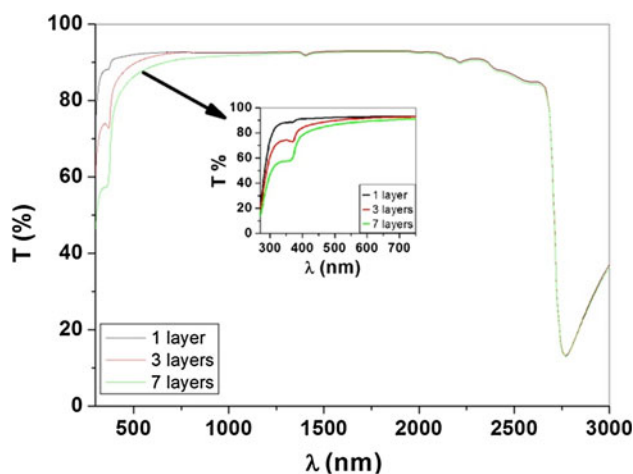


**Fig. 12** Optical transmission spectrum in the UV–VIS–NIR region of IZO coatings deposited on borosilicate substrates sintered in air at 600 °C with further annealing under reducing atmosphere for different layers



(doping concentration 1 atm.%) deposited on borosilicate glass, sintered in air at 600 °C in air. All layers exhibited a high transmission in the visible range (400–700 nm). The thicker the layer is, the less transmission due to the high absorption as shown in the inset of the Figure.

#### 4 Conclusion

Crystalline indium doped zinc oxide (IZO) nanopowders were synthesized using hydrothermal treatment processing. The doping concentration affected the phase structure as well as the shape of the nanopowders from nano rod-like structure to nanoparticulate one. The specific BET surface area increases with increasing the indium doping concentration. The energy gap is blue shifted by increasing the doping concentration related with a decrease in the crystallite size. The IZO nanoparticulate suspension has a zeta potential greater than 30 mV at pH = 6. Transparent conducting coatings made using redispersable IZO suspension were obtained. A sheet resistance as low as 35 k $\Omega_{\square}$  ( $\rho = 4.9 \times 10^{-3} \Omega.m$ ), and a transmission as high as 90 % were obtained. It is recommended to emphasize on the fact that the obtained result using nanoparticulate suspension for depositing IZO transparent conductive coatings needs more momentum in the process of the scientific experimenting and research and opens an interesting gate for the researchers in this field.

**Acknowledgments** One of the authors, Naji Al Dahoudi would like to thank the German academic exchange services (DAAD) for their financial support of his study visit at Leibniz institute of New Materials during summer 2012.

#### References

- Hotchandani S, Kamat PV (1992) *J Electrochem Soc* 119:1630–1634
- Sakohapa S, Tickazen LD, Anderson MA (1992) *J Phys Chem* 96:11086
- Harada K, Asakura K, Ueki Y, Toshina N (1992) *J Phys Chem* 96:9730
- Lee J, Hwang JH, Mashek TT, Mason TO, Miller AE, Siegel RW (1995) *J Mater Res* 10:2295
- Chou TP, Zhang Q, Fryxell GE, Cao G (2007) *Adv Mater* 19:2588–2592
- Hara K, Horiguchi T, Kinoshita T, Sayama K, Sugihara H, Arakawa H (2000) *Sol Energy Mater Sol Cells* 64:115
- Gao PX, Wang ZL (2005) *J Appl Phys* 97:044304
- Ko SC, Kim YC, Lee SS, Choi SH, Kim SR (2003) *Sens Actuators A* 103:130
- Sberveglieri G, Gropelli S, Nelli P, Tintinelli A, Giunta G (1995) *Sens Actuators B* 25:588
- Han JH, Kim DY (1998) *J Eur Ceram Soc* 18:765
- Shishiyance ST, Shishiyance TS, Lupan O (2005) *Sens Actuators B* 107:379
- Hachigo A, Nakahata H, Higaki K, Fujii S, Shikata S (1994) *Appl Phys Lett* 65:2556
- Morkoc H, Strite S, Cao GB, Lin ME, Sverdlov B (1994) *J Appl Phys* 76:1363
- Yi GC, Wang C, Park WI (2005) *Semicond Sci Technol* 20:S22
- Liu X, Wu X, Cao H, Chang RPH (2004) *J Appl Phys* 95:3141–3147
- Unalan HE, Hiralal P, Rupesinghe N, Dalal S, Milne WI, Amaratunga GAJ (2008) *Nanotechnology* 19:255608
- Li L, Meng G, Wang H, Zhai T, Fang X, Gautam U, Fang X, Bando Y, Golberg D (2011) *Chem Commun Camb* 47:8247–8249
- Kharisov BI (2008) *Recent Pat Nanotechnol* 2:190–200
- Jood P, Mehta RJ, Zhang Y, Peleckis G, Wang X, Siegel RW, Borca-Tasciuc T, Dou SX, Ramanath G (2011) *Nano Lett* 11:4337–4342
- Favier A, Muñoz D, Nicolás SMd, Ribeyron PJ (2011) *Sol Energy Mater Sol Cells* 95:1057–1061
- Bhosle V, Prater JT, Yang F, Burk D, Forrest SR, Narayan J (2007) *J Appl Phys* 102:023501
- Venkatesh PS, Ramakrishnan V, Jeganathan K (2012) *Cryst Eng Comm* 14:3907–3914
- Lin JM, Zhang YZ, Ye ZZ, Gu XQ, Pan XH, Yang YF, Lu JG, He HP, Zhao BH (2009) *Appl Surf Sci* 255:6460–6463
- Minami T, Sonohara H, Kakumu T, Takata S (1995) *Jpn J Appl Phys Part 2*:34
- Zhu BL, Zeng DW, Wu J, Song WL, Xie CS (2003) *J Mater Sci: Mater Electron* 14:521
- Liu P, Chou Y, Teng L (2009) *Appl Phys Lett* 94:242101
- Buonsanti R, Llordes A, Aloni S, Helms BA, Milliron DJ (2011) *Nano Lett* 11:4706–4710
- Tarasov K, Raccurt O (2011) *J Nanopart Res* 13:6717–6724
- Wang RP, Sleight AW, Cleary D (1996) *Chem Mater* 8:433
- Wang QL, Yang YF, He HP, Chen DD, Ye ZZ, Jin YZ (2010) *Nanoscale Res Lett* 5:882–888
- Li H, Zhang Y, Pan X, Zhang H, Wang T, Xie E (2009) *J Nanopart Res* 11:917–921
- Ahmad M, Zhao J, Iqbal J, Miao W, Xie Li, Mo R, Zhu J (2009) *J Phys D Appl Phys* 42:165406
- Maensiri S, Laokul P, Promarak V (2006) *J Cryst Growth* 289:102
- Wang XC, Chen XM, Yang BH (2009) *J Alloys Compd* 488:232
- Cuscó R, Alarcón-Lladó E, Ibáñez LAJ, Jiménez J, Wang B, Callahan MJ (2007) *Phys Rev B* 75:165202
- Umar A, Karunagaran B, Suh E, Hahn Y (2006) *Nanotechnol* 17:4072
- Chen KJ, Hung FY, Chang SJ (2009) *J Nanosci Nanotechnol* 9:3325
- Yang LW, Wu XL, Huang GS, Qiu T, Yang YM (2005) *J Appl Phys* 97:014308
- Reed JS (1988) *Introduction to the principles of Ceramic Processing*. Wiley and Sons, New York
- Parks GA (1965) *Chem Rev* 65:177–197